Deployable double layer tensegrity grid platforms for sea accessibility

Issam Hrazmi, Julien Averseng, Jérôme Quirant, Frédéric Jamin

Deployable double layer tensegrity grid platforms for sea accessibility

Issam Hrazmi*, Julien Averseng, Jérôme Quirant, Frédéric Jamin

LMGC, Univ. Montpellier, CNRS, Montpellier, France

Abstract

Tensegrity systems are a class of reticulated space structures composed of compressed bars maintained in equilibrium by a network of tensioned cables. Their stiffness depends both on elements' mechanical properties and their internal self-stress state. Taking advantage of their structural properties, we respond to the challenge of accessibility for everybody to the sea with a new concept of modular lightweight and deployable platforms. Variable configurations are developed to fit ecologically into the marine environment thanks to the transparency of double layer tensegrity structures. Moreover, allowing practical assembly and disassembly is considered in the design to respect the coastal law. Through a numerical study, we demonstrate in this paper the capability of this solution under various representative load cases and support conditions.

After the structural and design optimization of elements constrained by weight and stiffness, we detail the design of the nodes, which are the key components ensuring geometry and foldability of the structure. Finally, on-site setting and interfacing with ground supports is experimented in marine conditions to proof the feasibility of this concept.

Keywords:

sea accessibility, offshore platform, tensegrity, lightweight structures, deployable structures, modularity, node design

*Corresponding author

Email address: issam.hrazmi@umontpellier.fr (Issam Hrazmi)

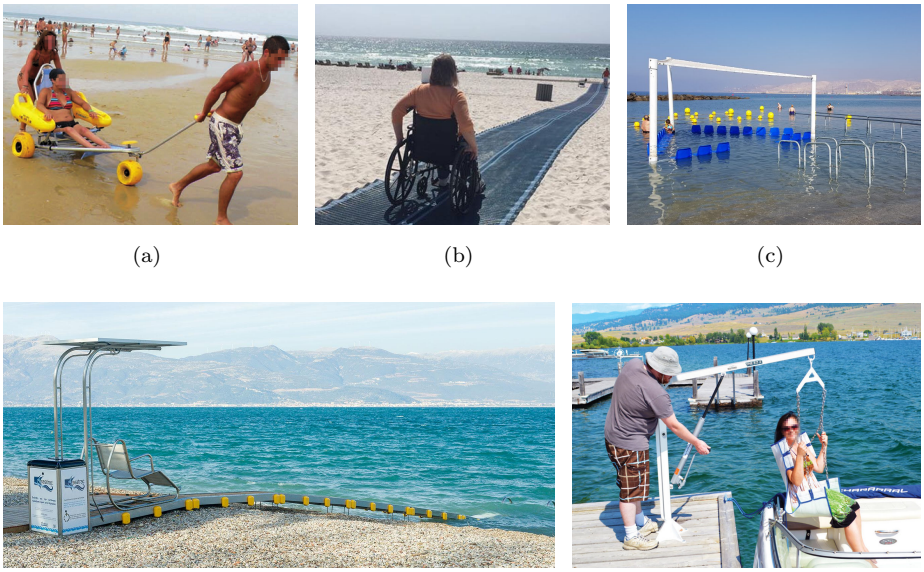

(a) (b) (c)

(d) (e)

Figure 1: (a) Amphibious wheelchair Tiralo®. (b) MobiMat® Tapiroul®. (c) Beach walkway system Baliser®. (d) Track mechanism SEATRAC®. (e) Pool lift AquaCreek®.

1. Introduction

To this day, access in complete autonomy to swimming areas is a laborious or impossible task for people with reduced mobility. Indeed, appropriate infrastructures are scarce and, when available, active intervention of a third party is needed. Being unable to leave their wheelchair while parked at water's edge, people with disabilities cannot enjoy swimming the way they should, like everyone else. This problem concerns too many people, nearly two million in the case of France [1].

In fact, the existing solutions for sea accessibility are limited. There exist beach mats or walkways that can help users get to water aside from keeping their wheelchairs (Fig. 1b,1c). Specific devices, such as amphibious wheelchairs, allow transfer in water, but they can be perceived as medical devices and requires assistance (Fig. 1a). Some solutions allow a wheelchair to be moved on a fixed track mechanism, but this only gives access to one person at a time (Fig. 1d). Pool lifts (Fig. 1e) can also be used to help people get into water but it needs to be fixed on supports above the water, which is not possible everywhere.

(a) (b)

Figure 2: (a) Pontoon of Pierre Caron (France). (b) Modular floating dock system Candock®.

Furthermore, solutions based on dock systems already exist and are serving also as accessibility platforms for people with reduced mobility (Fig. 2). For instance, one hospital in southern France has built permanent pontoon giving access to the beach for recreational activities, with limited assistance or full autonomy (Fig. 2a). Nevertheless, it can't be widespread due to littoral law restrictions and the permanent impact on the site. Floating solutions are another possibility but they are unsuitable on wavy waters like the sea and can be made of voluminous components (Fig. 2b).

To face these technical issues and in order to improve the inclusion and quality of life for people with reduced mobility, we engaged, in collaboration with a group of architects and the concerned public authorities, in the "Sea for Everybody" project. The aim is to provide a novel modular solution of platforms respecting the aesthetics and identity of swimming sites as well as the provisions of littoral law. Combined with motorized lifting system, these platforms allow a full autonomous access to water (Fig. 3b). This concept is intrinsically eco-friendly [2] and innovative through the combination of several constraints : modularity and adaptability, by allowing the assembly of modules in the form of clusters with any shape and depth; lightweightness, while ensuring stability and resistance; foldability, which is necessary for easy storage, handling and setting operations.

2. Structural concept

The designed and developed modular platforms in this project (Fig. 3b) consist of variable and expandable configurations, formed by juxtaposing [3]

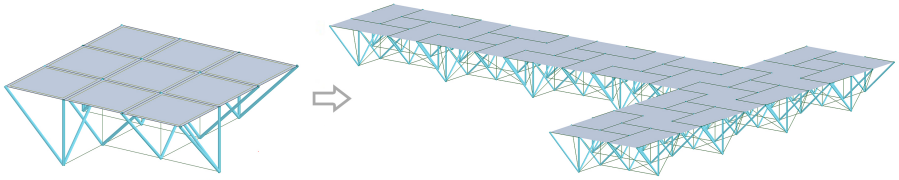

(a)

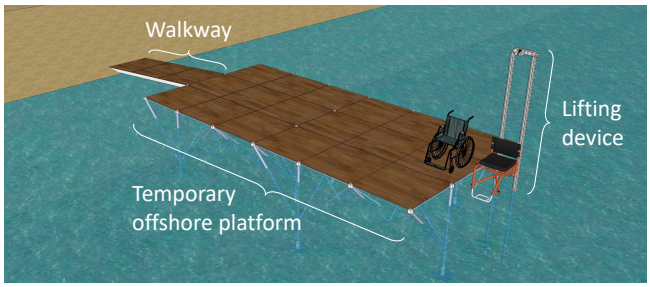

(b)

Figure 3: (a) Forming variable platforms from elementary tensegrity modules. (b) Overview of the "Sea for Everybody" project.

several elementary, rectangular and portable modules of limited size (Fig. 3a). The platform's structure is a double layer grid tensegrity system inspired from the "Tensarch" project [4, 5] that provided lightweight and modular structures (Fig. 4).

The concept of tensegrity emerged in mid-20th century in form of artworks, developed by researchers and architects [6, 7, 8, 9, 10]. It's a class of reticulated space structures composed of sets of compressed bars in self-equilibrium inside a continuous network of tensioned cables. Several studies are conducted worldwide on civil engineering applications, such as footbridges [11, 12, 13] and large roof structures [14].

Among the benefits of tensegrity, we can mention its potential for the realization of smart, adaptive [15, 16, 17, 18] and foldable structures [19, 20, 21], for which origami art can be a source of inspiration [22]. The stiffness and stability of a tensegrity structure depend both on the mechanical and geometrical properties of the elements, as well as their self-stress [23, 24], locally or globally distributed inside the structure. The self-stress design is carried out using form-finding methods [25, 26]. For "Tensarch" grid topology, self-stress is set

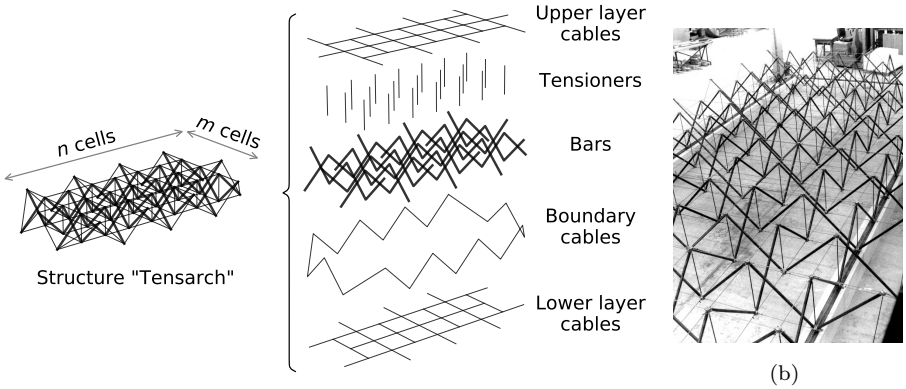

Figure 4: (a) Elements composing the "Tensarch" structure. (b) "Tensarch" 80 m^2 prototype.

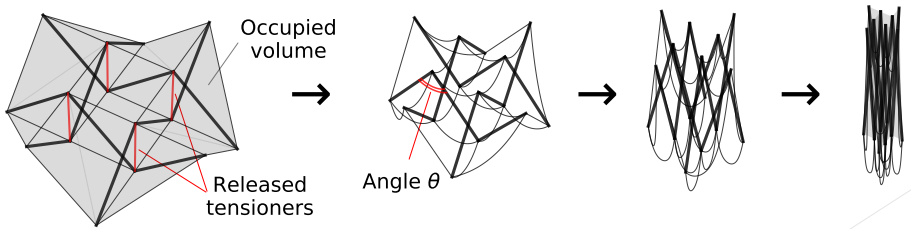

Figure 5: Folding process of a "Tensarch" module 3×3.

by shortening tensioners that are linking lower to upper layers (Fig. 4a).

The "Tensarch" topology can be seen at the local scale as a juxtaposition of "expanders" cells, which are V-shaped sets of bars in opposition linked around a vertical tensioner. Upper and lower layers appear like confinement plates for pentamode lattices [27], creating plane surface for displacement of people. In the absence of a self-stress state, by releasing only vertical tendons, the structure can be easily folded as a compact and handleable bundle (Fig. 5).

Length and width of these grids are multiples n and m of the chosen elementary cell dimensions, and cannot be less than 3 by 3, due to the specific boundary topology. The volume occupied in the deployed state is highly reduced by folding, i.e. up to 70% in the case of a module of 3×3 and 90% in the case of a module of 4×6. The Fig. 6 shows volume variation of different configurations $n \times m$ using a 1 m^3 cubic cell in function of the folding factor f, which depends on the angle θ between two linked bars, varying from 0 (folded)

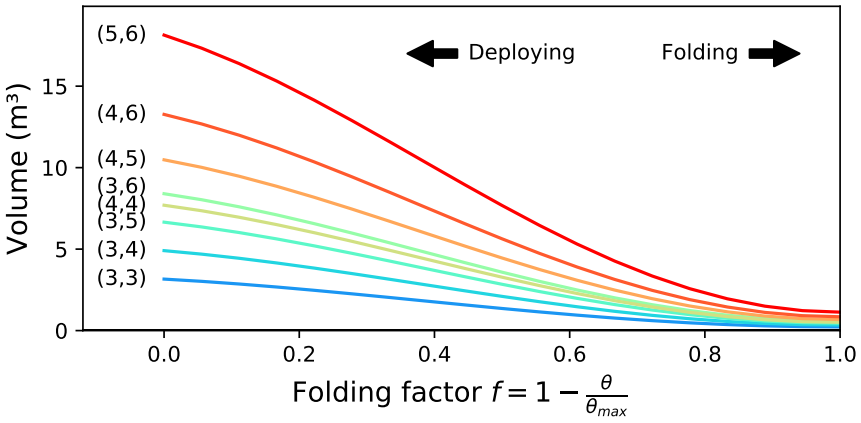

Figure 6: Volume occupied by "Tensarch" modules during folding and deployment process for a cell size of 1 m^3.

to θ_{max} (deployed, $\pi/2$ in this case).

In order to exploit this structure as a platform and to support vertical loads, surface deck elements must be fixed onto the upper layer nodes. As "Tensarch" topology provides only a part of the required nodes at the edges and corners, making appear cantilever areas, an additional isostatic system of brace and cable components is fixed on the adjacent lower nodes (Fig. 7), where forces can be redistributed in the structure [3].

Assembling many modules together, side by side, to form larger platforms, can be conducted by adding "sewing" elements, struts or tensioners, to connect nodes from both sides of modules in the assembly zone, depending on the supports conditions. The additional brace system is added afterwards at the border of the resulting structure before fixing the deck plates (Fig. 8).

Supports are composed of anchors threaded in the sand soil. Each one is connected to a lower layer node through an interface allowing vertical and horizontal adjustments. Number and positions of these supports are chosen so as to ensure the best stiffness and stability, while minimizing costly installation operations.

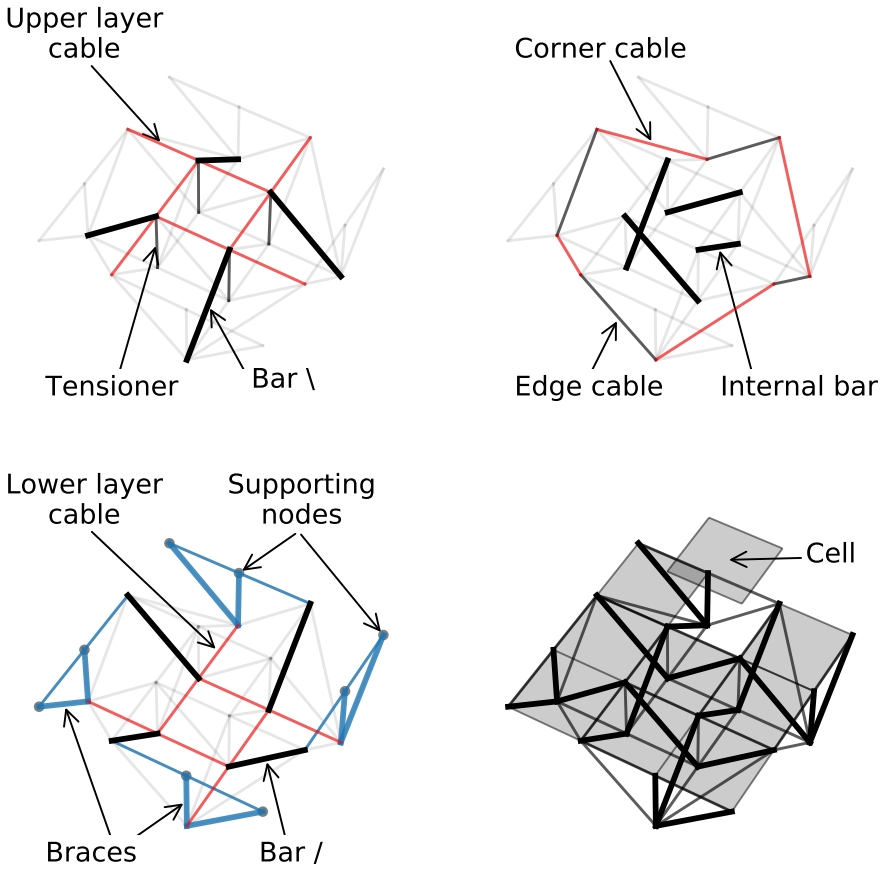

Figure 7: Composition of a single platform module 3×3.

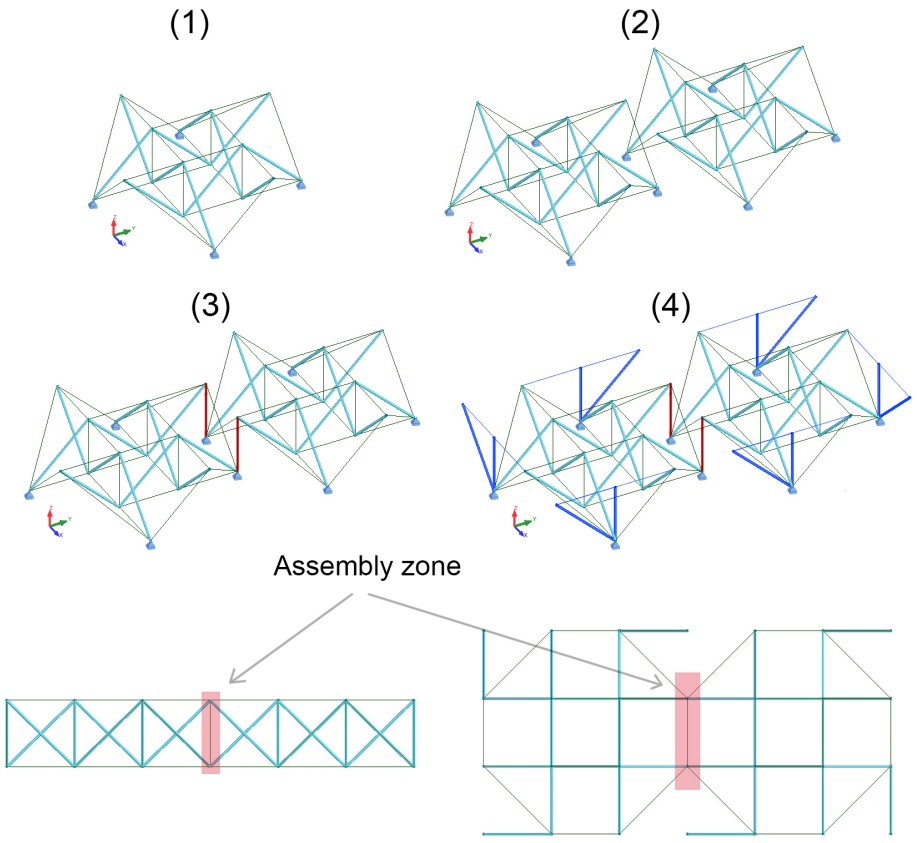

Figure 8: Assembling steps of two modules 3×3.

Elements	Materials	Young's modulus (GPa)	Elastic limit (MPa)	Poisson's ratio	Density (kg/m^3)	Geometry (mm)
Bar	Aluminium	71	240	0.3	2700	$D_{ext} = 40$, $t = 2$
Cable	Stainless steel	169	450	0.3	8000	$D = 10$
Plate	Wood	10	20	0.25	600	$t = 22$

Table 1: Mechanical and geometrical characteristics of the model.

3. Design and optimization

In order to assess the structural stiffness and stability of the proposed solution based on modular and deployable platforms, a numerical FEA model was built using ANSYS software [28]. As physical models had been built for experimenting foldability and assembly procedures, the mechanical and geometrical properties of elements in this model (Table 1) have been chosen in agreement with those of prototypes, allowing validation from experimental data.

3.1. Design criteria

For practical reasons, notably because the bundle size and weight in the folded state must be minimized, we chose to study platforms composed of elementary modules of 3 m × 3 m, thus proposing a minimum exploitable area of 9 m² and a low number of tensioners (Fig. 7). We propose to consider three dimensioning criteria that concern the buckling of bars, tension of cables and flexural displacement of deck plates.

3.1.1. Buckling limit of the bars

Due to their mechanical and geometrical properties as well as the type of their connection to the structure, bars might be subjected to the buckling phenomenon if their internal force exceeds a certain limit before their shape becomes unstable, called the buckling limit. It can be computed using few steps elaborated in the European standards Eurocode 3 [29]:

$$N_b \leq \chi \frac{A_b f_y}{\gamma_{M_1}} \tag{1}$$

Bars	L (mm)	N_{cr} (kN)	$\bar{\lambda}$	ϕ	χ	N_b (kN)
Vertical brace	854	41.5	1.17	1.36	0.49	28.2
Corner bar	1260	17.3	1.73	2.26	0.27	15.4
Internal bar	1290	17.7	1.77	2.34	0.26	14.8

Table 2: Numerical values of the buckling limit of the different bars' length.

where

- χ is the reduction coefficient, deduced from buckling laws, the slenderness and initial imperfections as:

$$\chi = \frac{1}{\phi + \sqrt{\phi^2 - \bar{\lambda}^2}} \tag{2}$$

where

$$\phi = 0.5(1 + \alpha(\bar{\lambda} - 0.2) + \bar{\lambda}^2) \tag{3}$$

and

$$\bar{\lambda} = \sqrt{\frac{A_b f_y}{N_{cr}}} \tag{4}$$

N_{cr} being the Euler buckling limit for the bar and $\alpha = 0.34$ a coefficient accounting for the initial imperfections;

- $A_b = 238.8$ mm^2 is the cross section of the bars;
- $f_y = 240$ MPa is the yield strength;
- $\gamma_{M_1} = 1$ is the safety factor.

3.1.2. Elastic limit of the cables

During service, cables may also be subjected to high internal forces that could lead to structural failure. To prevent this event, we set an elastic limit depending on the material and the cross section where the cables remain in the elastic behavior :

$$N_c \leq \frac{A_c f_y}{\gamma_{M_0}} \tag{5}$$

where

- $A_c = 50.3$ mm^2 is the cross section of the cables;
- $f_y = 190$ MPa is the yield strength;
- $\gamma_{M_0} = 1$ is the safety factor.

Thus, for all the cables' category, the tension should not exceed the value of 14.9 kN.

3.1.3. Serviceability bending limit of deck plates

As the deck plates are only subjected to non-permanent loads, the primary criterion concerns the deflection D of the elements, not their resistance. We must check that :

$$D \leq L/15000 \tag{6}$$

where L is the span of the plates.

3.2. Self-stress setting and design

In the "Tensarch" topology, the self-stress state in the deployed geometrical state is set by shortening its tensioners, which is sufficient to act on all the possible self-stress states. To ensure a homogeneous distribution when the platform is free of loads and simplify the parameters of this study, the same shortening is applied to all tensioners, which are 4 in this 3×3 configuration (Fig. 7). Thus, the distribution shape of internal forces is unique and, due to the high axial stiffness of elements and very low displacements induced, its level is quasi-linearly dependent on the imposed shortening (Fig. 9).

In consequence, the proportional relation between shortening and normal force is quasi constant for elements of the same category, due to structural symmetry (Fig. 10). Besides, with the given properties, the elastic limit of cables and the buckling limit of the bars occur for different self-stress levels. To ensure enough capacity for the intended application, while respecting all design criteria, the global shortening inducing initial self-stress must be chosen adequately.

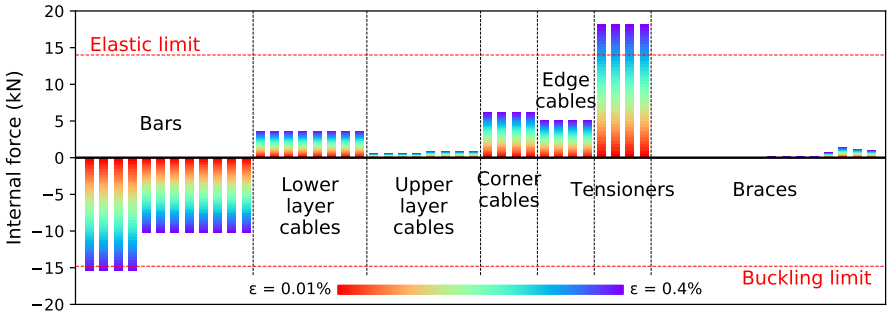

Figure 9: Spectrum of internal forces in the elements in function of self-stress state.

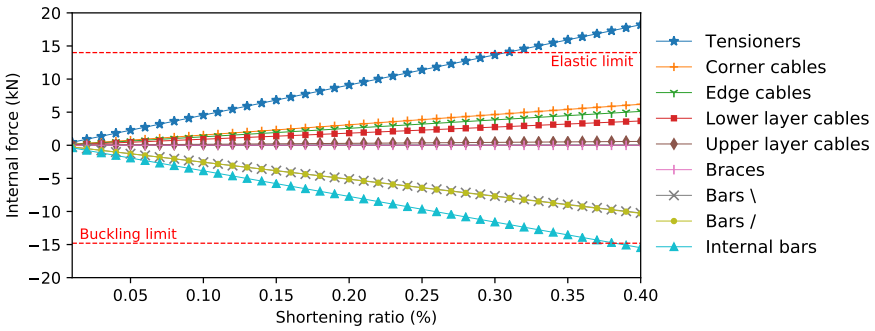

Figure 10: Evolution of internal forces in function of shortening ratio of the tensioners.

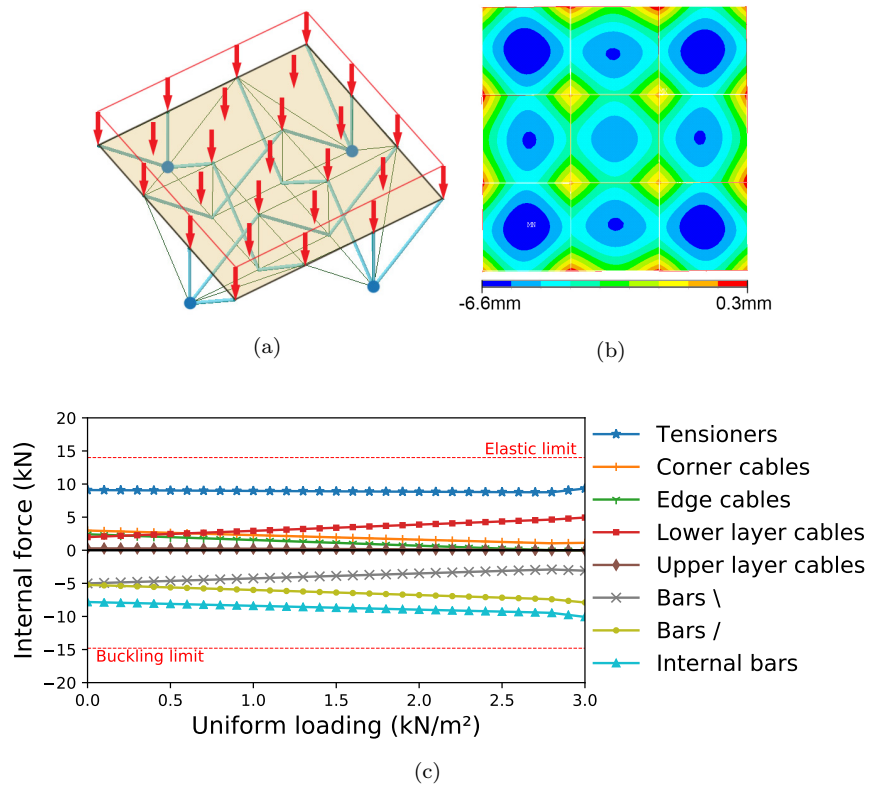

(a) (b)

(c)

Figure 11: (a) Illustration of a 3×3 module on 4 edge supports under uniform load case. (b) Vertical displacements maps of the deck plates under a loading of 3 kN/m^2. (c) Variation of internal forces in a 3×3 module as the load increases incrementally.

3.3. Response under uniform load

To validate the numerical approach, a simple case is simulated using a sequential and non-linear solving scheme. After installation of a self-stress state induced by a proposed 0.2% shortening, a uniform vertical load on the deck surface is applied, with values ranging from 0 to 3 kN/m^2 (Fig. 11a). As load increases, we observe, through the evolution of internal forces (Fig. 11c) and vertical displacements on the loaded deck plates (Fig. 11b), a non-linear behavior due to slackening of cables in the upper layer and redistribution of forces in the other elements, which occurs when the deck plates exceed a certain bending level. This behavior, typical for tensegrity systems, confirms the platform's stability and stiffness. It demonstrates also the validity of the numerical approach for use in parametric studies and structural optimizations.

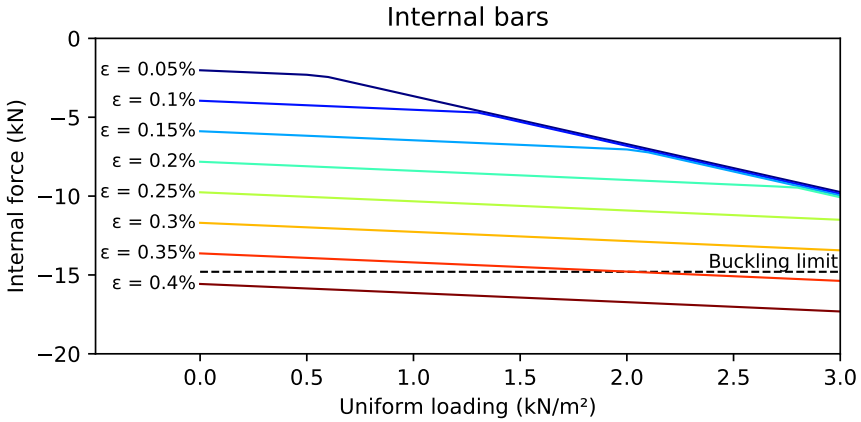

(a)

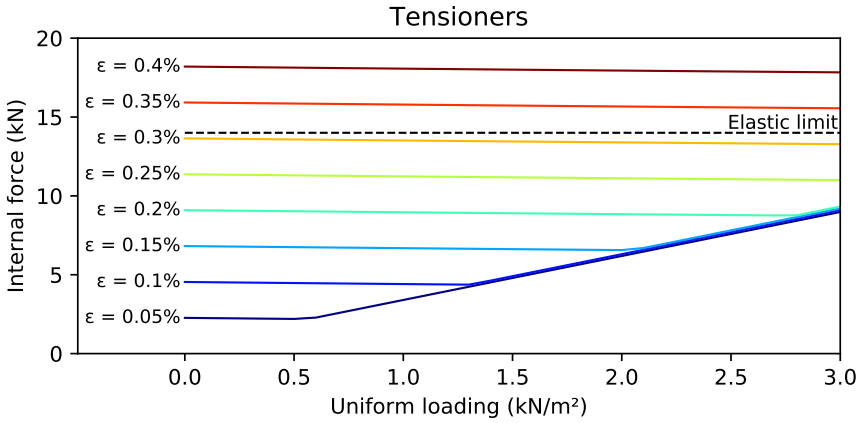

(b)

Figure 12: Internal forces in the internal bars (a) and the tensioners (b) in function of both the applied loading and the shortening ratio.

We can also see that the internal bars and tensioners are the most stressed elements and may exceed their predefined limits. In Fig. 12, we can see the evolution of internal forces in bars and tensioners under progressive loading and for different initial shortening ratio ϵ. For the design of self-stress, this graph confirms that a 0.2% shortening of the tensioners keep internal forces at a level of 65% of the elastic limit of cables and 52% of the buckling limit of the bars, giving safety margins for loaded situations up to 3 kN/m^2.

3.4. Optimization of supports conditions

As stability and stiffness of platforms of any configuration depend also on supports conditions, we compare here the structural responses for different sets of supports conditions, under a constant 3 kN/m^2 uniformly load, and for different platforms, composed of 1, 2 and 4 modules. As the number of supports and possible configurations multiply, risks of imprecision during the setting process increases, and consequently stability and stiffness of the platform. So, the goal is to minimize the setting operations while maintaining structural performances and safety.

3.4.1. One module platform

For a uniformly loaded platform made up of one module, we consider 3 supporting cases (Fig. 13a). Global stability is ensured in the case of edge supports (1st case) compared to the other cases where corners undergo relatively important displacement. It's also noted that in the 3rd case, some bars turn to be slightly compressed compared to the 1st and 2nd cases.

Considering those results and the different criteria, the 3×3 module has a better stability, stiffness and distribution of forces in the elements when it's supported by its 4 lower corner/edge nodes (1st case) (Fig. 13).

3.4.2. Platform of 2 modules

In the case of multi-modular platforms, an analogous analysis is performed with several support conditions cases, under the same loading, in order to minimize the total number of supports while ensuring an optimal performance.

Depending on the number s of shortlisted supports, the lower layer includes a set of 16 nodes, all candidate to support the platform in a way or another. Thus, there is $C_{16}^{s} = 16!/s!$ possible configurations (s-combinations) to do so. However, not all of them guarantee the optimal stability and rigidity. So, after eliminating trivial unstable configurations, only a few cases remains, of which only four are presented in Fig. 14a.

After analyzing and comparing the mechanical response of the platform for each supports configuration, it appeared that the global stability and rigidity of the platform can be ensured with the case N2.2, which requires only 7 supports and respects dimensioning criteria (Fig. 14b, 14c).

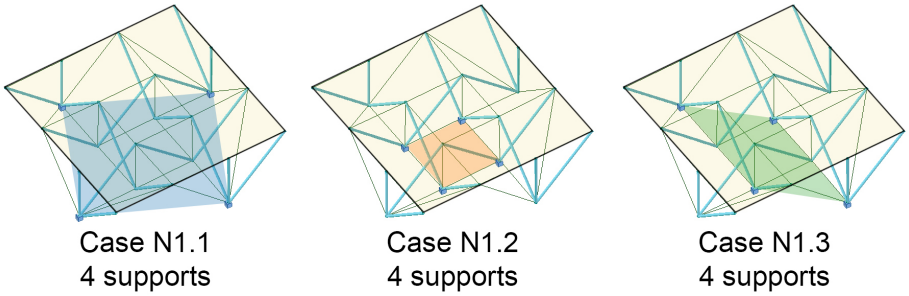

(a)

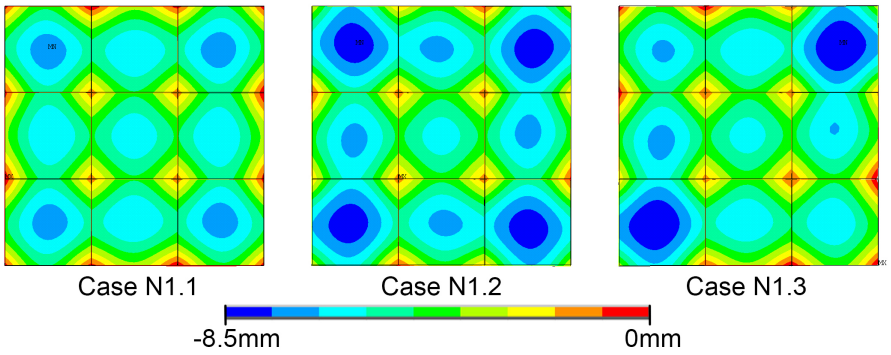

(b)

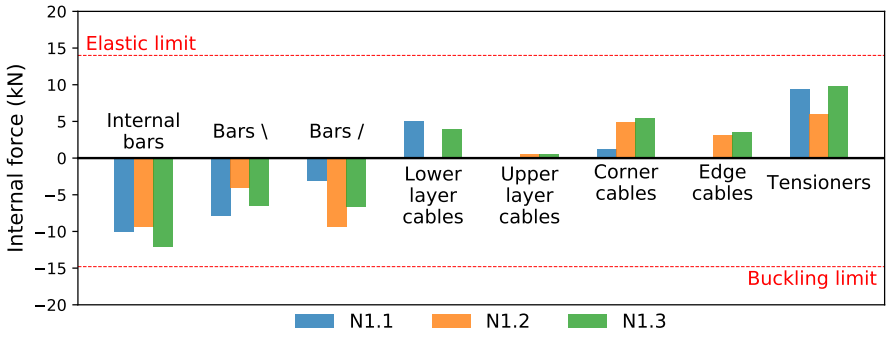

(c)

Figure 13: (a) Schemes of supports conditions of a platform of one module 3×3. (b) Vertical displacements maps of the deck plates. (c) Maximum values of internal force of different elements under a uniform loading of 3 kN/m^2.

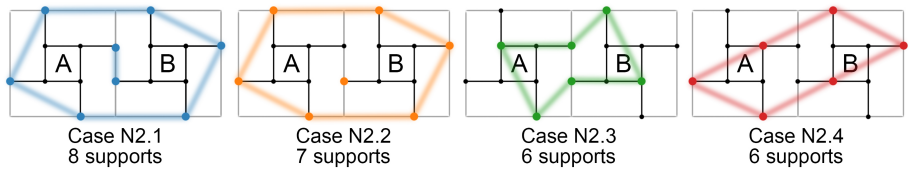

(a)

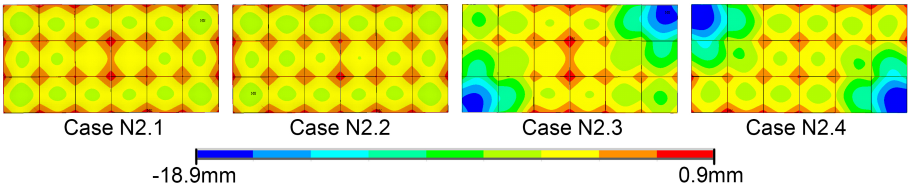

(b)

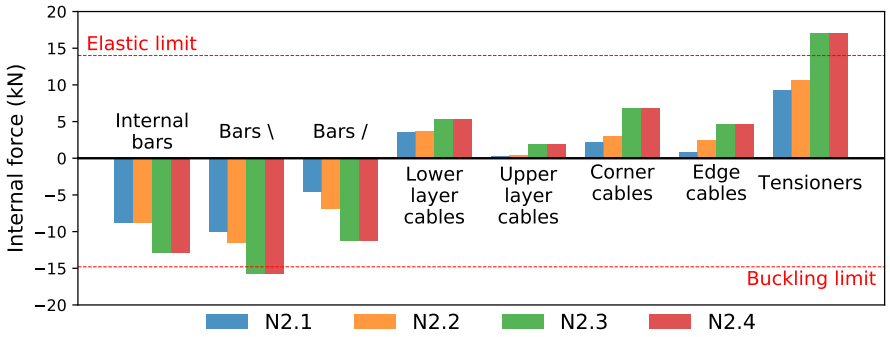

(c)

Figure 14: (a) Four typical supports schemes for a platform of two 3×3 modules. (b) Vertical displacements maps of the deck plates. (c) Maximum values of internal force of different elements under a uniform loading of 3 kN/m^2.

3.4.3. Platform of 4 modules

Similar analysis is conducted on a platform of 4 modules under the same load case (3 kN/m^2). With a set of 32 nodes in the lower layer, there are $C_{32}^{s} = 32!/s!$ different configurations to support the platform that depend on the chosen number of supports. However, we reduce here the analysis to 6 configurations (Fig. 15a). Instead of proposing a juxtaposition of individual conditions with 4 supports (like case N2.1 in Fig. 14), we aimed to further optimize the total number of the supports, using shared boundaries.

Vertical displacement in the deck plates is relatively important and exceeds the bending limit in the cases N4.3, N4.4 and N4.5 where at least 2 modules out of 4 use only 2 supports (Fig. 15b). Furthermore, the maximal internal forces in the elements exceed the limits in some bars and cables respectively for the same 3 supports configurations N4.3, N4.4 and N4.5 (Fig. 15c).

3.5. Variable loads

In operating conditions, the platform shall be subjected individually to several loads. In Fig. 17a, we consider 3 load cases: sea swell (L1), moving user in a wheelchair (L2), marine elevator (L3).
In the first load case (L1), being partially and permanently submerged, the platform is subjected to flowing water loads, which can be estimated by the Morison equation (7) [30] that describes the inline force on a cylindrical element fixed body in oscillatory flow.

$$dF = \frac{1}{2} C_D \rho D v|v| dz + C_M \rho \frac{\pi D^2}{4} \dot{v} dz \tag{7}$$

where

- $C_D = 1$ and $C_M = 2$ are respectively the drag coefficient and the inertia coefficient;
- D is the diameter of cylinder;
- $\rho = 1050$ kg/m^3 is the sea water density;
- v and $\dot{v}$ are respectively the flow velocity and the flow acceleration; where the flow velocity of shallow waters is expressed by the linear wave theory

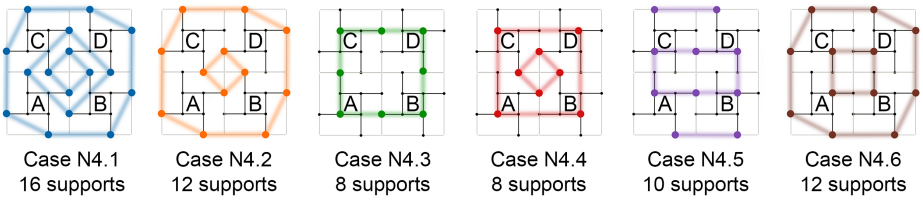

(a)

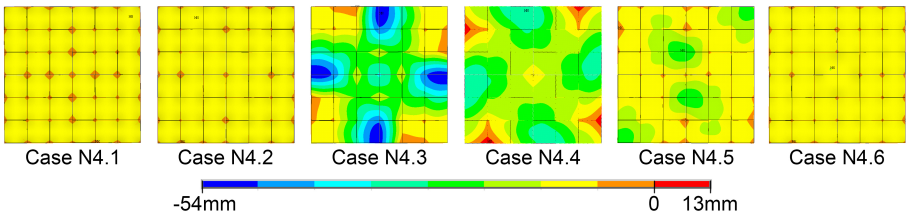

(b)

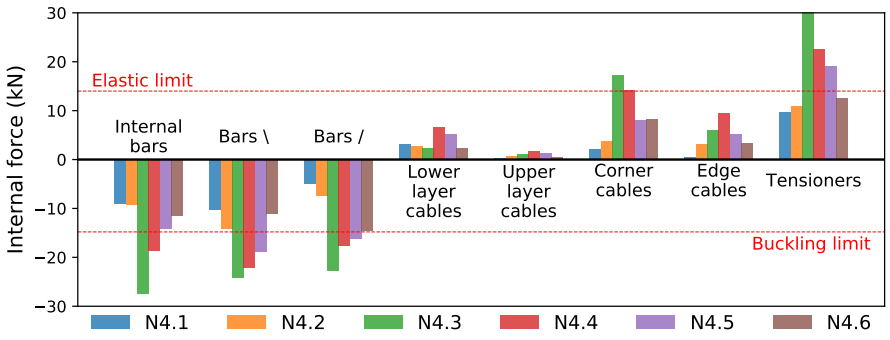

(c)

Figure 15: (a) Different schemes of supports conditions of a platform of four modules 3×3. (b) Vertical displacements maps of the deck plates. (c) Maximum values of internal force of different elements under a uniform loading of 3 kN/m^2.

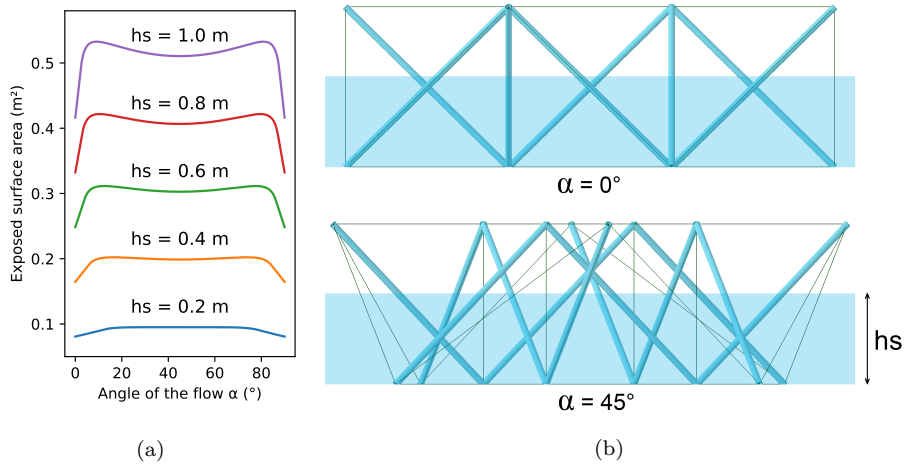

(a) (b)

Figure 16: (a) Exposed surface area of a module 3×3 for different submerged heights hs. (b) Illustrations of a submerged module 3×3 viewed from different angles.

as follow:

$$v = \frac{agk}{\omega} \frac{\cosh(k(z+d))}{\cosh(kd)} \cos(kx - \omega t) \tag{8}$$

- $d = 1.5$ m is sea depth;
- $a = 1$ m is wave amplitude;
- $g = 9.81$ m/s^2 is gravity acceleration;
- $k = 2\pi/\lambda$ is wave number, $\lambda = 10$ m is wave length;
- $\omega = \sqrt{kg \tanh(kd)}$.

However, given that structure's transparency towards the flow depends both on its direction, expressed by α, and the submerged height hs (Fig. 16), the net wave load is a function of the previous parameters and its value is brought in this simulation to lower layer nodes. As we carry in this study only static analysis, we consider for this load case the effective value due to its oscillatory nature.

The analysis shows that wave loads (L1) have only slight impact on internal forces of lower layer cables thanks to the structure's transparent aspect (Fig. 17b), while no impact on deck plates stability is noticed.

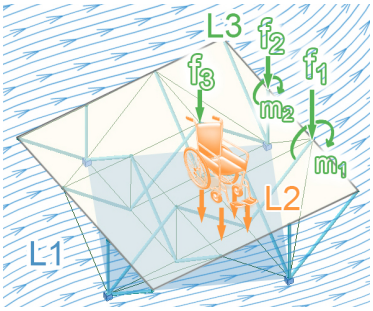

(a)

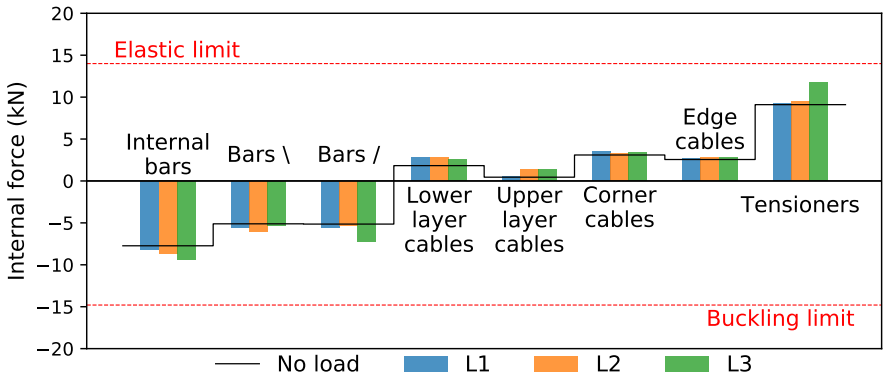

(b)

Figure 17: (a) Illustration of a 3×3 module platform subjected to 3 different load cases. (b) Maximum values of internal force of different elements under 3 load cases.

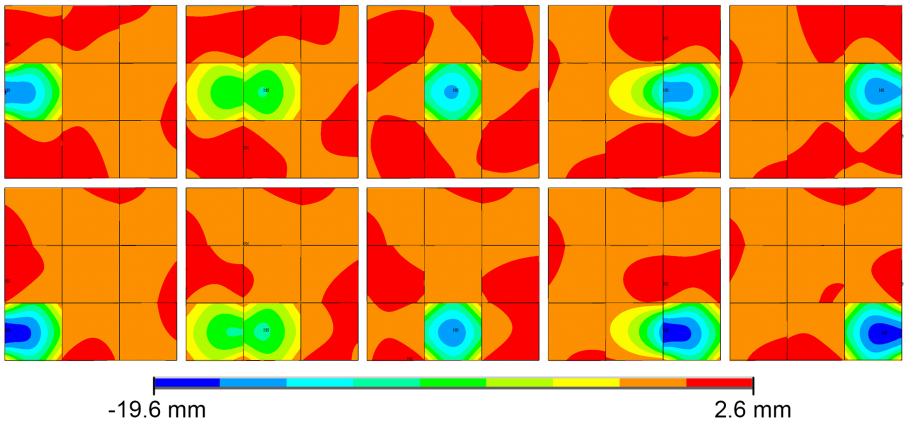

Figure 18: Vertical displacements maps of a moving wheelchair on the middle and edge of a 3×3 module platform in 5 steps.

For the second load case (L2), we consider a vertical force of 2 kN distributed on 4 contact points to model a moving wheelchair in straight lines on the middle and edge of a 3×3 module platform.
Maximum values of internal force of all family of elements, for different wheelchair positions, are considered in this analysis and they show no significant change compared to the unloaded case (Fig. 17b). In terms of displacement, the wheelchair has a localized impact on the underneath deck plates that does not compromise the global stability of the platform (Fig. 18).

In the third load case (L3), the elevator is fixed on platform's edge and modelled by 3 vertical forces and 2 moments ($f_1 = 2$ kN, $f_2 = f_3 = 1$ kN, $m_1 = 2$ kN.m and $m_2 = 1$ kN.m).
The mechanical response shows that elevator's weight has a relatively significant effect, especially on tensioners and bars (Fig. 17b).

4. Mechanical design of the nodes

Besides its optimal mechanical performance, stability and stiffness of the upper layer, the topology of "Tensarch" structures offers other assets, such as lightweightness, transparency, foldability and modularity. The key components ensuring the different functions are the nodes.
To make this possible, their design should take into consideration different constraints, namely allowing folding mechanisms, convergence of forces and their

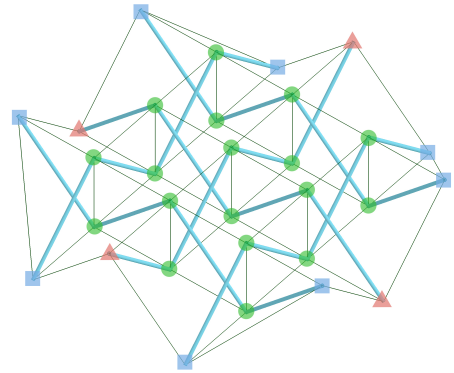

(a) "Tensarch" module 4×4.

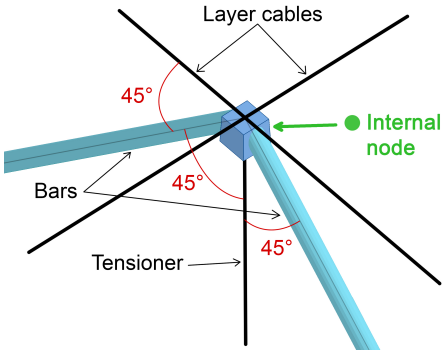

(b) Internal node (circle).

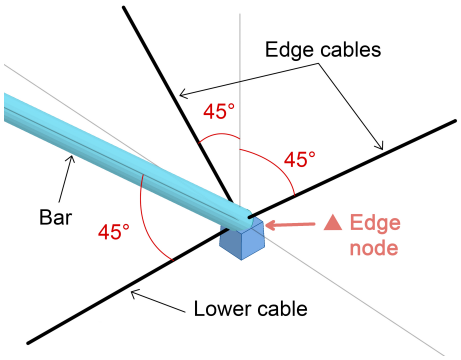

(c) Edge node (triangle).

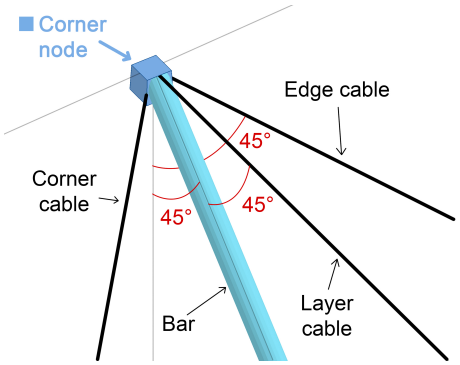

(d) Corner node (square).

Figure 19: Different types of nodes of a "Tensarch" module 4×4.

transmission through the structure at the deployed state. In addition, nodes' design must provide easy manufacturing, assembly process and connectivity to other modules, additional bracing elements, surface elements and supports.

4.1. Nodes

A module of $n \times m$ has a total of $2(n \times m - 1)$ nodes occupying different positions. However, thanks to a certain level of symmetry and the relational configuration materialized by the incidence and number of elements supported by each node, it is possible to reduce the number of nodes to 3 main categories: internal nodes (Fig. 19b), edge nodes (Fig. 19c) and corner nodes (Fig. 19d).

For practical reasons, especially to avoid congestion due to the number of elements that can be connected by certain nodes (Table 3), node' body is designed under a solid modeling computer-aided design [31] with two parts: one for the

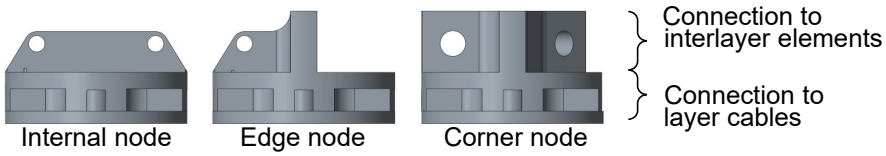

Figure 20: Body parts for the 3 categories of nodes.

	Layer cables	Inter-layer cables	Tensioners	Bars
Internal node	4	0	1	2
Edge node	1	2	0	1
Corner node	1	2	0	1

Table 3: Number and type of connected elements per node class.

connection to interlayer elements and the other for connecting layer cables. As all nodes are joining layer cables, the latter is then designed in the same way for the 3 categories of nodes (Fig. 20).

Furthermore, to ensure connectivity between nodes and cables at their ends, nodes are designed considering 3 types of crimping solutions used for the 3 categories of cables used in the structure, which are boundary cables (Fig. 21a), layer cables (Fig. 21b) and tensioners (Fig. 21c).

For ergonomic reasons, with a crimped fillister at their ends, the layer cables are simply "trapped" into the main node body then covered with a hood fixed with screws (Fig. 22).

For interlayer elements, the joints' axes are precisely positioned to avoid potential congestion between different elements during folding and to guarantee the convergence of internal forces at the deployed state.

For bar elements, a hollow cross-section is adopted due to its relatively high

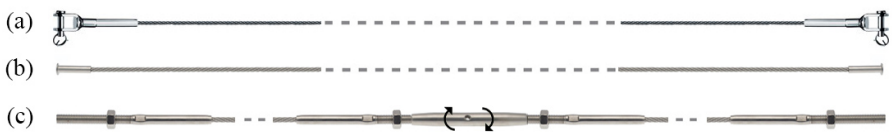

Figure 21: (a) Cable with crimped clevis fastener (boundary cables) – (b) Cable with crimped fillister at its ends (layer cables) – (c) Couple of cables with crimped threaded rods at ends and assembled with a turnbuckle (tensioners).

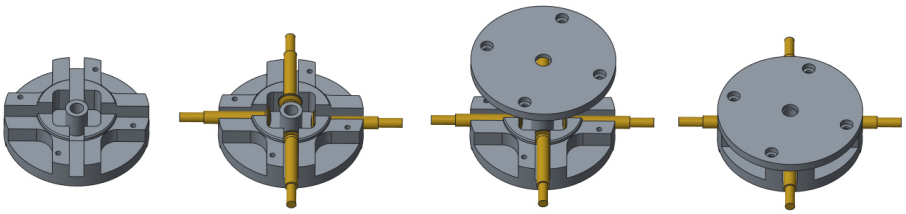

Figure 22: Connection to layer cables.

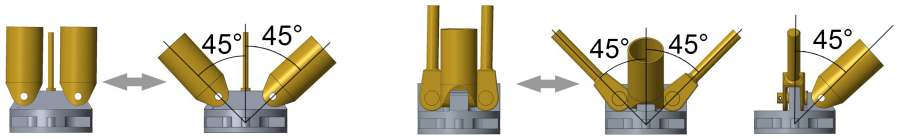

(a) Internal node.

(b) Edge node.

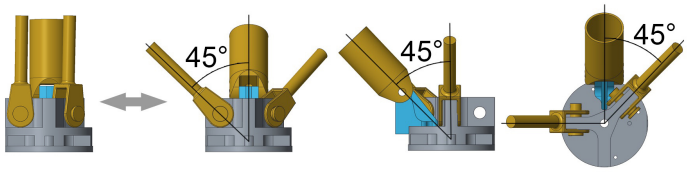

(c) Corner node.

Figure 23: Visualization of incidence angles of the connected interlayer elements and their folding mechanisms at each node of the structure.

moment of inertia. Its connection with the node body is ensured by a clevis, which allows the rotation mechanism necessary to the folding and deployment process, all while respecting the incidence angles at the deployed state (Fig. 23).

4.2. Deck plates support

For its usage as a multi-purpose platform, deck plates are fixed on upper layer nodes from their corners via a specific interface allowing vertical support and in-plane restrain and fixed on the hood (Fig. 24). The presence of theses deck plates brings flexural stiffness to the structure but also block the shear finite mechanisms.

4.3. Link with ground supports

In order to preserve marine environment, the solution of the platform foundations we opted for is based on Skrew^{TM} anchor [32] that can be fixed in

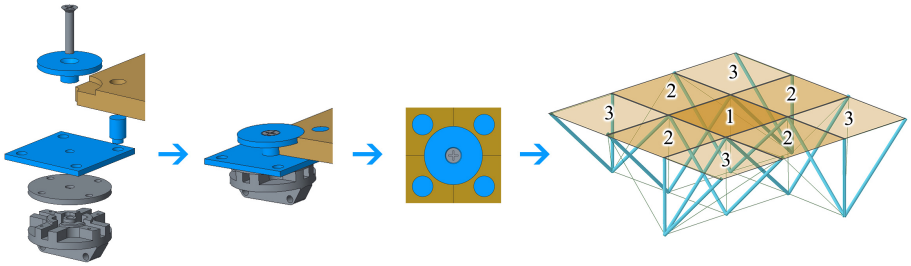

Figure 24: Assembling strategy of the deck plates.

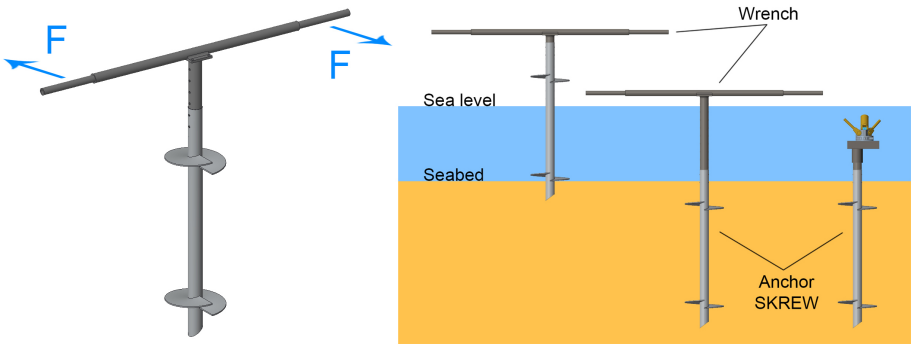

Figure 25: Adapted anchor Skrew^{TM} for the support solution.

the seabed using a wrench specially designed for the operation (Fig. 25). This lightweight screw-pile solution is characterized by its minimal environmental impact, its stability and resistance to high forces [33, 34, 35], axially and laterally.

Once the concerned area is enclosed, the implantation is carried out using a triangulated bracing system to guide Skrew^{TM} anchors and ensure approximately, given the rough conditions, the distances between supports before and after implantation. A linking system between the anchor and respective support node allows final distance adjustments from 1 to 2 cm (Fig. 25).

5. Experimental work

Besides the structural role of all the components, as seen in section 4, their mechanical design takes also into account constraints including ease of assembly and practicality of machining process. Furthermore, to ensure an effortless assembling, high accuracy is needed and obtained in our case with CNC milling.

After assembling all the components, the structure can be folded into a bundle or deployed by introducing the required self-stress state for the intended

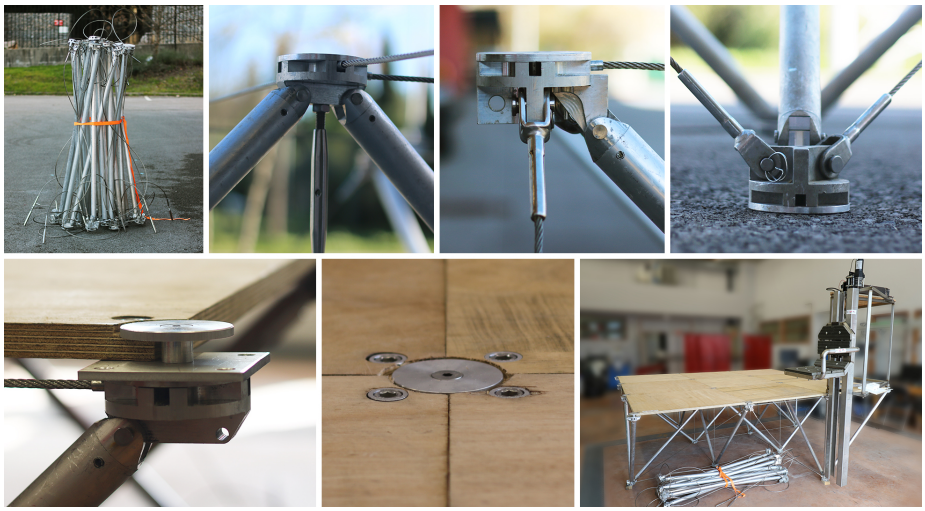

Figure 26: Assembly of the prototype's components.

use by spinning equally turnbuckles to shorten the tensioners. Then the deck plates are easily fixed thanks to the ergonomically designed interface. The elevator, one of the important devices of the solution, is then fixed afterwards allowing users to get into the water with full autonomy. A fully assembled module 3×3 prototype with 9 deck plates and an elevator prototype is presented in Fig. 26.

In order to cover a given surface area, the "Tensarch" structure offers the possibility to either use one module regardless of the dimensions as long as the surface concerned is rectangular and no weight limitation is imposed. It is also possible to assemble multiple, smaller elementary modules in order to generate complex surfaces. This is also practical, making use of lightweight modules. For example, a 3 m×3 m prototype offers 9 m^2 of covered surface area for approximately a weight of 25 kg.

Furthermore, the design of nodes and the standardization of components in this "Tensarch" topology makes possible resizing a given module, by adding one or several rows of nodes and components to each side, thus extending or reducing the covered surface area (Fig. 27).

In Fig. 28, folding and deployment process and modularity are demonstrated by assembling two 3×3 modules to obtain 18 m^2 of covered surface area. Then the 2 modules are merged to make a module 5×3 which is resized to obtain a

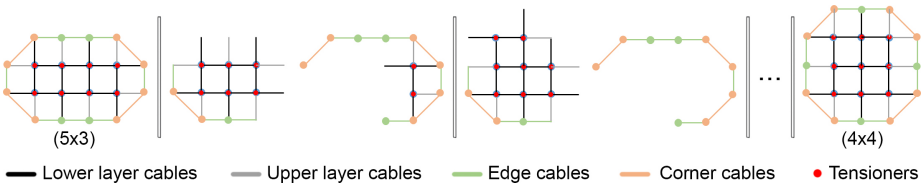

Figure 27: Scheme of reconfiguration steps from a module 5×3 to a module 4×4.

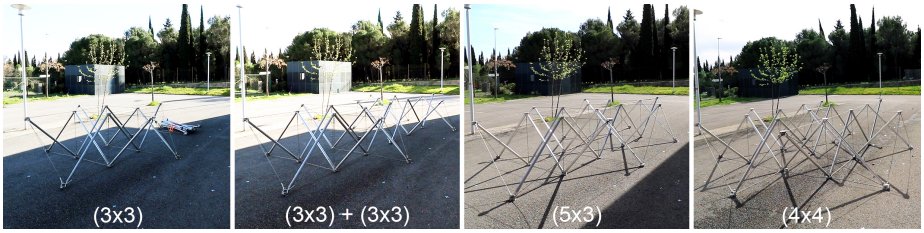

Figure 28: Modularity and reconfiguration demonstration.

module 4×4, thus covering finally the area of 16 m² (1 m² mesh size).

Preliminary tests have also been carried out in real conditions on a coastal site during a few hours (Fig. 29). The purpose was to test the implantation system of one module platform in the first instance, but also to time and evaluate the difficulty of the whole setting process. It took finally one hour to setup the platform but only half an hour to remove it. The difference in timing is mainly due to the implantation process of the ground supports, which requires precision and attention to details. However, the deployment of the grid and fixing of deck plates is a quick operation. Further experimentations are expected soon with improved procedures in order to optimize the implantation process, which is crucial for stiffness, stability and performance of the platform.

6. Conclusion

The mechanical properties offered by tensegrity structures, such as lightweightness, foldability, modularity and stiffness, have given birth to a solution of platform for sea accessibility. As an outcome of the ambitious project "Sea for Everybody", in combination with a lifting device, this solution aims to bring people with reduced mobility an access to swimming areas with full autonomy. These platforms answer to weight, simplicity of usage and serviceability constraints, while being exploitable in isolated areas with a minimal environmental

Figure 29: Deployment and in-situ tests of a prototype of one module 3×3 – Villeneuve-lès-Maguelone (France).

impact.

A numerical model has been built, allowing to establish a self-stress design methodology and performing predictive analyses. We demonstrated that with this right self-stress state, taking account of the elements mechanical capabilities, the mechanical behavior of the platform is appropriate for accessibility purpose as it provides stability and stiffness under service and environmental loads. An optimization of the supports conditions was also conducted to minimize the impact and cost of installation operations.

For the concretization of such a solution, a heavy work of mechanical design has been conducted. The folding constraints combined with the internal forces equilibrium conditions, milling capabilities and modularity led to a practical solution using only three different structural nodes. These components allow building structural modules of any size, retrofiting and recycling. Simplicity was also a concern for ensuring its usage in real conditions by coastal site communities.

The in-situ tests carried out so far have shed lights on practicality during the first stages of the setup process, namely the assembly, transportation and deployment but also the possibility of reconfiguration of the modules' in-plane geometry. However, it was showed that the implantation of supports in marine environment is a tough task to consider in a complementary study.

Thus, further work will focus on the implantation system for ease of use and for a better precision of anchors position. Modularity between modules with

different heights is also the next subject of experimentation, as this solution is also adaptable to the elevation profile of the seabed in particular. And finally, attention will be devoted towards durability of the used materials in marine environment.

Declaration of Competing Interest

The authors declare that they have no known competing financial interests or personal relationships that could have appeared to influence the work reported in this paper.

Acknowledgements

This work was conducted through the financial support of the French Region Occitanie, Nîmes Métropole and University of Montpellier.

References

[1] N. Chautard, Habitats insalubres et situations de handicap, Editions de l'Espérou, 2002-2003.

[2] I. Hrazmi, J. Averseng, J. Quirant, F. Jamin, Double layer tensegrity grid offshore plateform for sea accessibility, in: IASS Annual Symposium 2019 – Form and Force, Barcelona, Spain, 2019.

[3] F. Jamin, J. Quirant, J. Averseng, S. Devic, Assembly of foldable tensegrity modules, WO2017194775A1 (2017).

[4] R. Motro, Tensarch : A tensegrity double layer grid prototype, 2002, pp. 57–66. doi:10.1680/ss5v1.31739.0007.

[5] V. Raducanu, R. Motro, Stable self-balancing system for building component, WO2002081832A1 (2002).

[6] F. R. Buckminster, Tensile-integrity structures, US3063521A (1962).

[7] D. G. Emmerich, Construction de réseaux autotendants, FR1377290 (Sep. 1964).

[8] K. D. Snelson, Continuous tension, discontinuous compression structures, US3169611A (1965).

[9] R. Motro, Tensegrity: Structural Systems for the Future, Elsevier Science, 2003.

[10] V. Gomez-Jauregui, Tensegrity Structures and their Application to Architecture, 2010.

[11] L. Rhode-Barbarigos, N. B. Hadj Ali, R. Motro, I. F. C. Smith, Designing tensegrity modules for pedestrian bridges, Engineering Structures 32 (4) (2010) 1158–1167. doi:10.1016/j.engstruct.2009.12.042.

[12] N. Veuve, S. Dalil Safaei, I. F. C. Smith, Active control for mid-span connection of a deployable tensegrity footbridge, Engineering Structures 112 (2016) 245–255. doi:10.1016/j.engstruct.2016.01.011.

[13] J. Feron, I. Bouckaert, P. Mengeot, J. Van Steirteghem, P. Latteur, Influence of random loads on the optimal design of tensegrity footbridges, in: Proceedings of IASS Annual Symposia, Vol. 2019, International Association for Shell and Spatial Structures (IASS), 2019, pp. 1–8.

[14] R. Panigrahi, A. Gupta, S. Bhalla, Dismountable steel tensegrity grids as alternate roof structures, Steel and Composite Structures 9 (05 2009). doi:10.12989/scs.2009.9.3.239.

[15] N. Veuve, A. C. Sychterz, I. F. C. Smith, Adaptive control of a deployable tensegrity structure, Engineering Structures 152 (2017) 14–23. doi:10.1016/j.engstruct.2017.08.062.

[16] F. Fraternali, E. De Chiara, R. E. Skelton, On the use of tensegrity structures for kinetic solar facades of smart buildings, Smart Materials and Structures 24 (2015) 105032. doi:10.1088/0964-1726/24/10/105032.

[17] A. Graells Rovira, J. M. Mirats Tur, Control and simulation of a tensegrity-based mobile robot, Robotics and Autonomous Systems 57 (5) (2009) 526–535. doi:10.1016/j.robot.2008.10.010.

[18] A. P. Sabelhaus, J. Bruce, K. Caluwaerts, P. Manovi, R. F. Firoozi, S. Dobi, A. M. Agogino, V. SunSpiral, System Design and Locomotion of SUPERball, an Autonomous Tensegrity Robot, in: 2015 IEEE International Conference on Robotics and Automation, Seattle, Washington, 2015.

[19] S. Pellegrino, Deployable Structures, Springer, 2001. doi:10.1007/978-3-7091-2584-7.

[20] V. Gomez-Jauregui, M. Quilligan, C. Manchado, C. Otero, Design, Fabrication and Construction of a Deployable Double-Layer Tensegrity Grid, Structural Engineering International 28 (2018) 13–20. doi:10.1080/10168664.2018.1431379.

[21] A. Pizzigoni, A. Micheletti, G. Ruscica, V. Paris, S. Bertino, M. Mariani, V. Trianni, S. Madaschi, A new T4 configuration for a deployable tensegrity pavilion, in: Proceedings of IASS Annual Symposia, Vol. 2019, International Association for Shell and Spatial Structures (IASS), 2019, pp. 1–6.

[22] R. Miranda, E. Babilio, N. Singh, F. Santos, F. Fraternali, Mechanics of smart origami sunscreens with energy harvesting ability, Mechanics Research Communications 105 (2020) 103503. doi:https://doi.org/10.1016/j.mechrescom.2020.103503.

[23] K.-I. Kawaguchi, Y. Hangai, S. Pellegrino, H. Furuya, Shape and Stress Control Analysis of Prestressed Truss Structures, Journal of Reinforced Plastics and Composites 15 (12) (1996) 1226–1236. doi:10.1177/073168449601501204.

[24] S. Amouri, J. Averseng, J. Quirant, J.-F. Dubé, Structural design and control of modular tensegrity structures, European Journal of Environmental and Civil Engineering 19 (6) (2015) 687–702. doi:10.1080/19648189.2014.965849.

[25] J. Quirant, N. M. Kazi-Aoual, R. Motro, Designing Tensegrity Systems : The case of a double layer grid, Engineering Structures 2003 (n°25) (2003) 1121–1130. doi:10.1016/S0141-0296(03)00021-X.

[26] A. G. Tibert, S. Pellegrino, Review of Form-Finding Methods for Tensegrity Structures, International Journal of Space Structures 18 (4) (2003) 209–223. doi:10.1260/026635103322987940.

[27] A. Amendola, G. Carpentieri, L. Feo, F. Fraternali, Bending dominated response of layered mechanical metamaterials alternating pentamode lattices and confinement plates, Composite Structures 157 (2016) 71–77. doi:10.1016/j.compstruct.2016.07.031.

[28] ANSYS Inc, Mechanical APDL R2 (2019).

[29] J. Morel, Calcul des structures métalliques selon l'Eurocode 3, Eyrolles, 2005.

[30] J. R. Morison, J. W. Johnson, S. A. Schaaf, et al., The force exerted by surface waves on piles, Journal of Petroleum Technology 2 (05) (1950) 149–154.

[31] PTC, Creo Parametric 3.0 M190.

[32] Sea Tech and Fun Europe, Skrew^{TM}.

[33] Y. Chen, A. Deng, A. Wang, H. Sun, Performance of screw-shaft pile in sand: Model test and DEM simulation, Computers and Geotechnics 104 (2018) 118–130. doi:10.1016/j.compgeo.2018.08.013.

[34] F. M. Abdrabbo, A. Z. El Wakil, Laterally loaded helical piles in sand, Alexandria Engineering Journal 55 (4) (2016) 3239–3245. doi:10.1016/j.aej.2016.08.020.

[35] A. Mohajerani, D. Bosnjak, D. Bromwich, Analysis and design methods of screw piles: A review, Soils and Foundations 56 (1) (2016) 115–128. doi:10.1016/j.sandf.2016.01.009.